ion activities of Cu^{2+}, Zn^{2+}, Co^{2+}, and Mn^{2+} were computed from metal ions–NTA equilibriums as described by W. G. Sunda, D. W. Engel, and R. M. Thuottle [*Environ. Sci. Technol.* **12**, 409 (1978)]. Computed free ion activities based on added metal concentrations are: Cu, $10^{-13.3}M$ to $10^{-9.8}M$; Zn, $10^{-10.3}M$; Co, $10^{-10.3}M$; and Mn, $10^{-9.5}M$.
12. Gravid females of the mud crab were collected near Beaufort, North Carolina. They were kept in tanks of running seawater and transferred to culture bowls when their eggs were ready to hatch. Newly hatched larvae were then reared at 27.5°C in 8-cm (diameter) culture bowls containing 50 ml of metal-buffered seawater with ten zoeae per bowl. There were five replicates for each $\{Cu^{2+}\}$. Larvae were transferred to clean bowls with fresh media and fed newly hatched *Artemia* nauplii daily.
13. Lyophilized *Rhithropanopeus harrisii* larvae were rehydrated and homogenized in 0.2*M* tris-HCl, *p*H 7.4, with an acid-washed Teflon pestle tissue grinder. The homogenate was centrifuged at 100,000*g*, and the resulting supernatant was filtered by centrifugation through a 0.2-μm nylon filter. A 100-μl portion of the filtered cytosol was chromatographed on a HPLC gel permeation column (Toyo Soda TSK SW 3000) at 1 ml/min with 0.25*M* tris-HCl, *p*H 7.4. Fractions (1 ml) were collected, and copper concentrations were determined by atomic absorption spectrophotometry (Perkin-Elmer 5000) with a graphite furnace (HGA 500). The coefficient of variation was 7.56 percent for copper-thionein.
14. This metal-binding ligand (i) bound zinc, copper, and cadmium; (ii) was induced by elevated $\{Cu^{2+}\}$; (iii) had a low absorption at 280 nm, suggesting a lack of aromatic amino acids; (iv) co-migrated (HPLC) with a scorpion-fish metallothionein that had previously been characterized by amino acid analysis (unpublished data); and (v) had a DEAE elution profile similar to that of metallothioneins that have been characterized in other species of crab (*10*). Final confirmation of this ligand as metallothionein, however, awaits amino acid analysis.
15. Survival [mean ± standard error (S.E.)] for five replicates each at the seven $\{Cu^{2+}\}$ data points: $x = 72.3 \pm 8.9$ percent; $F = 1.18$; d.f. = 6,28; $P = 0.25$. Duration: $x = 10.6 \pm 0.16$; $F = 1.25$; d.f. = 6,28; $P = 0.25$.
16. A. R. D. Stebbing, *Aquat. Toxicol.* **1**, 227 (1981); *J. Mar. Biol. Assoc. U. K.* **61**, 35 (1981).
17. R. B. Laughlin, Jr., J. Ng, H. E. Guard, *Science* **211**, 705 (1981); B. M. Sanders and J. D. Costlow, *J. Therm. Biol.* **6**, 357 (1981).
18. Our seven data points were fitted by a derivative-free nonlinear regression program, in *BMDP Statistical Software*, W. J. Dixon, Ed. (Univ. of California Press, Los Angeles, 1981), p. 305. This program also calculates asymptotic standard deviations of parameter estimates. For copper-thionein: $Y_{max} = 101.4 \pm 7.4$ μmole/kg; $A = 50.8 \pm 4.2$ μmole/kg; $k = 1.6 \times 10^{-11} \pm 9.83 \times 10^{-12}M$; $n = 2.12$; r^2 (coefficient of determination) = 0.9804. For cytosolic copper: $Y_{max} = 176.8 \pm 18.4$ μmole/kg; $A = 74.6 \pm 10.1$ μmole/kg; $k = 1.78 \times 10^{-11} \pm 1.267 \times 10^{-11}M$; $N = 2$; $r^2 = 0.9613$.
19. Supported by the Office of Health and Environmental Research, Ecological Division of the Department of Energy and the Ocean Assessment Division, National Ocean Services, NOAA. We thank D. Brown, S. George, D. Manahan, and G. Roesijadi for reviewing earlier drafts of this manuscript; R. Burri and T. Marshall for technical assistance; and D. Bradley for statistical assistance.

7 March 1983; revised 27 May 1983

Catch a Falling Star: Meteorites and Old Ice

Abstract. *A model for the process of meteorite concentration in blue ice regions of the Antarctic ice sheet is proposed based on data from near the Allan Hills and the assumptions that both meteorite influx and glacial flow have been constant. The meteorite influx is calculated to be 60 × 10^{-6} kilogram per square kilometer per year, and the age of the exposed ice to be 0 to 600,000 years, varying with distance from the Allan Hills. These results are in line with other estimates of influx rate and with measurements of the terrestrial ages of the meteorites, providing support for the assumption of steady flow and meteorite influx. This may be the oldest sequence of ice in stratigraphic order yet discovered, and the results imply that this part of the east Antarctic ice sheet has been approximately steady during this time interval.*

There are places on the Antarctic ice sheet where meteorites are found in large numbers. Ordinarily meteorites become buried in the snow, incorporated in the ice, carried to the edge of the continent (*1*), and discharged into the sea. In special places, however, the ice does not reach the sea but evaporates or otherwise ablates at the surface, and the meteorites are exposed. These collect at the ablating surface where they are joined by direct falls. Compressive ice flow, characteristic of ablation zones, further concentrates meteorites.

Steady-state meteorite fall rate and steady-state glacial flow are assumed. Meteorites that fall onto the accumulation zone (Fig. 1) attain a concentration inside the ice given by $\gamma = f/A_c$, where f represents the meteorite infall rate (mass per unit area per unit time) and A_c the snow accumulation rate expressed in meters of ice equivalent per year. This concentration does not depend on depth or age since we take both f and A_c as constant in both time and position. Thus the meteorites are uniformly distributed inside the ice sheet along the flow line leading to the ablation zone.

Three mechanisms concentrate meteorites. Those that are buried in the accumulation zone reappear in the ablation zone (*2*) at a rate γA_b, where A_b represents the rate of ice loss—in the case of the Allan Hills region, loss is mainly by evaporative sublimation. These meteorites are joined by direct falls at rate f. Finally, ablation zones usually show compressive flow, such that the area between three or more points on the ice surface becomes smaller with time. This affects the meteorite concentration (M), which is expressed in mass of meteorites per unit area. Let $\dot{\varepsilon}_s$ represent the sum of the two horizontal strain rates at the surface; then by adding the three effects, the time-rate of surface concentration is

$$\frac{dM}{dt} = \gamma A_b + f - \dot{\varepsilon}_s M \qquad (1)$$

Since the strain rate $\dot{\varepsilon}_s$ is on average negative, all three terms contribute to increasing M. For ice flow, expressions are obtained for $\dot{\varepsilon}_s(x)$ and $t(x)$, where x is horizontal position along the flow line. Then this equation is solved for $M(x)$, our objective.

Assume that the glacier has been steady—that is, its geometry and velocity have not changed with time. Then the shape of the glacier, the rates of accumulation or ablation at the surface, and ice movement are related to one another by continuity. In our case we need consider only the ablation zone

$$Z\,\overline{\frac{dx}{dt}} = -\int_0^x (Z\bar{\dot{\varepsilon}}_y + A_b)\,dx \qquad (2)$$

where x represents distance from the lower end of the glacier (the snout), $Z(x)$ ice thickness, and $\bar{\dot{\varepsilon}}_y$ the strain rate for flow-line spreading (positive) or convergence (negative) in map view. Both the velocity, $\overline{dx/dt}$, and the lateral spreading, $\bar{\dot{\varepsilon}}_y$, are expressed as means through the ice thickness, but Eq. 1 calls for surface values. The surface velocity, dx/dt_s, and surface spreading, $\dot{\varepsilon}_{ys}$, are larger

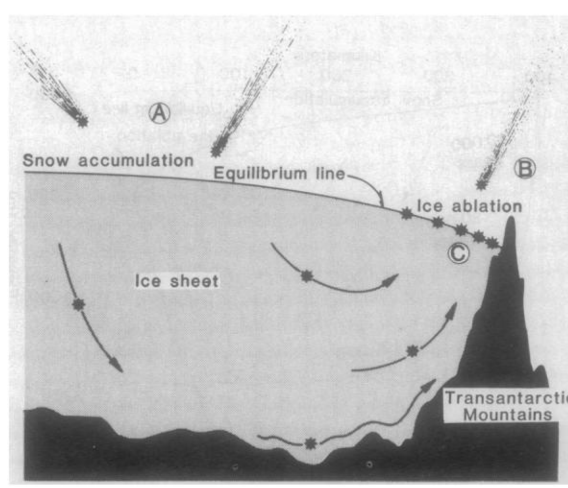

Fig. 1. Profile of an ice sheet and mechanisms for concentration of meteorites. (A) Meteorites fall into the snow accumulation zone and are transported to the ablation zone by ice flow; (B) meteorites fall directly onto ablation zone; and (C) compressive ice flow "crowds" meteorites together. Vertical exaggeration, approximately ×50.

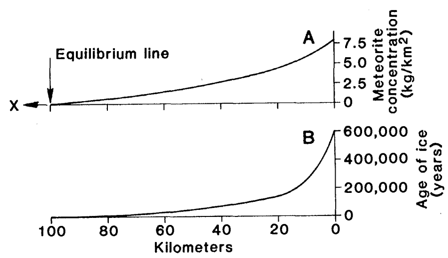

Fig. 2. As a function of distance from the lower end of the ice sheet, (A) meteorite concentration (with an infall rate of 60×10^{-6} kg/km² per year) and (B) age of the exposed ice.

than the mean values by a factor ϕ (*3*), which is usually in the range 1.2 to 1.5. Let us substitute

$$\frac{dx}{dt_s} = -\frac{\phi}{Z}\int_0^x \left(\frac{Z\,\dot{\varepsilon}_{ys}}{\phi} + A_b\right) dx \qquad (3)$$

It is not necessary to consider flow in the snow accumulation zone of the glacier, and this is convenient because there are few data for that region.

The expression in Eq. 3 is applicable to places like the Allan Hills meteorite area, where the glacier ends on land. In places like the Yamato Mountains, where meteorites have also been concentrated (*2*), some of the ice continues out to sea. In such cases the origin of x would be defined for a site where the ice flux $Z\,\overline{dx/dt}$ can be specified and included in the equation of continuity.

The strain rate $\dot{\varepsilon}_s$ is the sum of the lateral spreading, $\dot{\varepsilon}_{ys}$, and the velocity gradient along the flow line

$$\dot{\varepsilon}_s = \dot{\varepsilon}_{ys} + \frac{d}{dx}\left(\frac{dx}{dt_s}\right) \qquad (4)$$

This is used with Eqs. 2 and 3 to eliminate time (t) and solve for $M(x)$.

The results are plotted in Fig. 2, and relevant parameters are listed in (*4*). The calculated maximum meteorite concentration is $(0.14 \times 10^6$ years$)f$ (*5*). As of 1981, 623.7 kg of meteorites have been found in a 75 km² area near the Allan Hills (8.3 kg/km²), suggesting average value for the meteorite infall rate of about 60×10^{-6} kg of meteorites per square kilometer per year. More small meteorites no doubt will be found, but they will not affect this calculation significantly. Fewer meteorites have been found at greater distances from the Allan Hills, as the model predicts, but they have not yet been systematically collected.

During the last 200 years, estimates of infall rate (*6–8*) have been based on numbers of observed falls, which are associated with recovery of specimens. These estimates may be revised upward by factors that depend on seasonal (×1.5) and diurnal (×2) variations in recovery rates (*7*), diurnal variation in meteoroid influx rate (×2) (*9*), and various sociological (×2) and geographic (×7) factors (*10*). Existing estimates based on numbers of falls therefore differ by a factor of 84 (1.5 × 2 × 2 × 2 × 7), depending on which correction factors are chosen. The Antarctic collections have the advantages of independence from observed fall statistics and from questions of the magnitude of correction factors due to seasonal and diurnal variations, as well as virtual independence from the problem of incomplete recovery. Antarctic meteorite data also represent an integration of the rate of fall over a much greater time period.

Limitations on our method are mainly due to uncertainties in the ice flow model and inherent statistics in meteorite infall rate. The ice flow model suffers from a lack of sufficient field data.

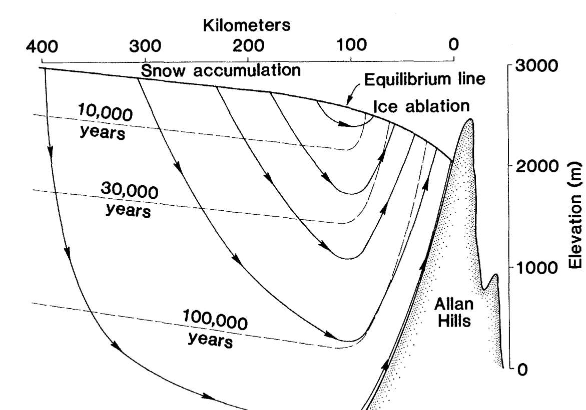

Fig. 3. Profile of the ice sheet near the Allan Hills showing ice flow trajectories (solid lines) and isochrones or time lines. Vertical exaggeration, about ×100.

Our model assumes constant accumulation and ablation rates and steady glacial flow while in the model of Nishio and others (*11*) the ice sheet is proposed to have thinned by a large amount. They studied crystal size and orientation of ice near the snout and assumed that retrograde metamorphic effects were negligible and hence that ice had traveled to a maximum depth of only 500 m. From this they calculate the ice to be only 20,000 years old and suggest large past changes in ice sheet size and perhaps meteorite influx in order to explain the observed meteorite concentration and the terrestrial ages, which are discussed later. We do not agree with this interpretation. The bubbles in the ice are arranged in planes (*11*) and seem to be formed by exsolution from the ice. Air is fully or mostly dissolved in ice at a depth of 1100 m (*12*), and the Allan Hills ice must have traveled deeply as we have modeled it.

Ice trajectories and isochrones are shown in Fig. 3. The isochrones show the age of ice, and therefore the terrestrial age of the contained meteorites, and these ages become greater as the ice and meteorites are carried toward the snout. At any site in the ablation zone, a range of terrestrial ages for the meteorites is expected: the oldest ages belong to meteorites that traveled long distances in the glacier, and younger ages are associated with direct falls onto the blue ice. The older meteorites appear at the surface nearer the snout and are rarer because less old ice is being exposed than young ice. Measured terrestrial ages of Allan Hills meteorites are in the range of 0 to 700,000 years (*13*), which is in approximate agreement with ages in Fig. 3. This agreement supports the approximately steady flow concept, at least for as long as the oldest measured terrestrial age (*14*).

The ablation zone exposes, in stratigraphic order, ice ranging in age from 0 to 600,000 years. The maximum age of the ice, and the meteorites, is very sensitive to the variation with depth of ice velocity that is used in the calculation. This is not known for this area, and a model like that used for Byrd Station, West Antarctica (*15*), is used. However, even for the most conservative model of no variation with depth (all motion by bottom sliding), the age near the glacial snout is 200,000 years—still very old.

A possible complication would arise if the ice is folded or overthrust; in that case the simple stratigraphic succession would be disturbed. We observed a large number of dust bands during a visit to the region. These have not yet been closely analyzed, but they are probably windblown dust or perhaps tephra layers from nearby volcanoes and must originate in the snow accumulation zone. They dip upglacier as expected and occur close to, as well as at least 30 km from, the ice front. Some bands show small-scale concentration variations, which may be expected from deposition around sastrugi ("snow dunes") or within ripple troughs. Because of this and because they contain only very fine material in nearly uniform bands they are not considered to be Thule-Baffin moraines. The dust bands that crop out can be traced, and no offsets or folds were found. The bands are exposed farther down-glacier in valleys in the ice surface, as expected from faster flow between obstacles in the glacial bed. The continuity and form of the dust bands support our simple model for ice flow and indicate that the ice is in stratigraphic order.

The calculations suggest that this part of the ice sheet has been approximately steady for some 600,000 years, during a time when other glaciers waxed and waned dramatically. There is also probably a long stratigraphic record of ice exposed near the Allan Hills. What this ice and its contained air and impurities will reveal about past changes in climate, ice sheet flow, atmospheric composition, and volcanic activity is yet to be determined. Such a record is without parallel and is intermediate in character between the more detailed but shorter term ice core records and the coarser sea floor and palynologic records.

I. M. WHILLANS
Department of Geology and Mineralogy and Institute of Polar Studies, Ohio State University, Columbus 43210
W. A. CASSIDY
Department of Geology and Planetary Science, University of Pittsburgh, Pittsburgh, Pennsylvania 15260

References and Notes

1. E. J. Olsen, *Nature (London)* **292**, 516 (1981).
2. T. Nagata, in *Proceedings of the Second Symposium on Yamato Meteorites*, T. Nagata, Ed. (Memoirs of National Institute of Polar Research, Tokyo, Japan, 1978), special issue 8, p. 70.
3. I. M. Whillans, *J. Glaciol.* **18**, 359 (1977).
4. A_c = 0.039 m/year [measured in the central portion of the ice sheet (*16*); average value for entire accumulation zone is probably within a factor of 2 of this value]. A_b = 0.06 m/year [measured in the 10 km nearest the Allan Hills (*17*); probably within a factor of 2 of the average value for the entire ablation zone]. ϕ = 1.3 [from (*3*), not critical for influx calculations]. Position of equilibrium line is 100 km on the basis of the limit of blue ice on Landsat images and is probably accurate to 50 percent. Drewry (*18*) shows a very short flow line for the ice leading to the Allan Hills. Our observations on slopes and the deformation of dust bands lead us to conclude that the flow line is hundreds of kilometers long, as we have modeled it. $Z = 0.6x^{3/4}$ with Z and x in meters [empirical fit to radio echo–determined ice thicknesses (*10*)]. For $x > 100$ km, Z = 3400 m. For $\dot{\varepsilon}_{ys} = |dx/dt|_s/R$, R = 100 km for $x < 100$ km and $R = \infty$ for $x > 100$ km (R is radius of curvature of elevation contours for ice flowing in direction of maximum slope).
5. About 60 percent of the meteorites have been transported through the glacier. Concentrations are increased by 25 percent at the snout because of the third mechanism, the effect of which is much less important farther inland.
6. G. S. Hawkins, *Astron. J.* **65**, 318 (1960).
7. H. Brown, *J. Geophys. Res.* **65**, 1679 (1960).
8. ———, *ibid.* **66**, 1316 (1961).
9. D. W. Hughes, in *Solid Particles in the Solar System*, I. Halliday and B. A. McIntosh, Eds. (Symposium 90, International Astronomical Union, Paris, 1980), p. 207.
10. H. T. Millard, *J. Geophys. Res.* **68**, 4297 (1963).
11. F. Nishio, N. Azuma, A. Higashi, J. O. Annexstad, *Ann. Glaciol.* **3**, 222 (1982).
12. A. J. Gow and T. Williamson, *J. Geophys. Res.* **80**, 5101 (1975).
13. E. L. Fireman, L. A. Rancitelli, T. Kirsten, *Science* **203**, 453 (1979); J. C. Evans, and L. A. Rancitelli, *Smithson. Contrib. Earth Sci.* *23* (1980), p. 45; K. Nishiizumi, J. R. Arnold, D. Elmore, X. Ma, D. Newman, H. E. Gove, *Earth Plant. Sci. Lett.* **62**, 407 (1983).
14. D. J. Drewry, *Nature (London)* **287**, 214 (1980).
15. I. M. Whillans, *J. Glaciol.* **24**, 15 (1979).
16. J. M. Palais, I. M. Whillans, C. Bull, *Ann. Glaciol.* **3**, 239 (1982).
17. F. Nishio and J. O. Annexstad, in *Proceedings of the Fifth Symposium on Antarctic Meteorites*, T. Nagata, Ed. (Memoirs of National Institute of Polar Research, Tokyo, Japan, 1980), special issue 17, p. 1.
18. D. J. Drewry, in *Antarctic Geoscience*, C. Craddock, Ed. (Univ. of Wisconsin Press, Madison, 1982), p. 947.
19. We thank J. Bolzan, R. Hooke, D. Hughes, and M. van Heeswijk for helpful comments. Supported by NSF grants DPP-7821104A02 and DPP-7920824. Contribution 466 of the Institute of Polar Studies.

29 July 1982; revised 10 May 1983

Eccentric Ringlet in the Maxwell Gap at 1.45 Saturn Radii: Multi-Instrument Voyager Observations

Abstract. *The Voyager spacecraft observed a narrow, eccentric ringlet in the Maxwell gap (1.45 Saturn radii) in Saturn's rings. Intercomparison of the Voyager imaging, photopolarimeter, ultraviolet spectrometer, and radio science observations yields results not available from individual observations. The width of the ringlet varies from about 30 to about 100 kilometers, its edges are sharp on a radial scale < 1 kilometer, and its opacity exhibits a double peak near the center. The shape and width of the ringlet are consistent with a set of uniformly precessing, confocal ellipses with foci at Saturn's center of mass. The ringlet precesses as a unit at a rate consistent with the known dynamical oblateness of Saturn; the lack of differential precession across the ringlet yields a ringlet mass of about 5 × 10^18 grams. The ratio of surface mass density to particle cross-sectional area is about five times smaller than values obtained elsewhere in the Saturn ring system, indicating a relatively larger fraction of small particles. Also, comparison of the measured transmission of the ringlet at radio, visible, and ultraviolet wavelengths indicates that about half of the total extinction is due to particles smaller than 1 centimeter in radius, in contrast even with nearby regions of the C ring. However, the color and brightness of the ringlet material are not measurably different from those of nearby C ring particles. We find this ringlet is similar to several of the rings of Uranus.*

Images of Saturn's rings obtained by the Voyager cameras showed several eccentric features, including an elliptical ringlet in an otherwise clear gap at about 1.45 Saturn radii (*1, 2*) which is now called the Maxwell gap. In addition, we now have occultation studies of this feature at several wavelengths. Voyager 1 carried out a microwave occultation with the dual-frequency spacecraft transmitter as a source and reception on the ground (*3*); on Voyager 2, the star δ-Scorpii was observed by the ultraviolet spectrometer (UVS) (*4*) and the photopolarimeter (PPS) (*5*) as it was occulted by the rings. We briefly discuss these observations and draw conclusions regarding (i) the size of the ring particles, (ii) the distribution of material within the ringlet, and (iii) the total mass. Derived quantities are compared with other ring features.

The most detailed Voyager images of ring C had resolution of about 5 to 7 km per line pair (*1, 2*). The photometric brightness and the optical depth from the stellar occultation determine that the particle visible reflectivity is 0.26. This is indistinguishable from the surrounding material; we find no significant difference in particle color or particle albedo between this feature and surrounding C ring, in contrast with earlier reports (*6*).

The radio occultation experiment measured the rings' optical depth at wavelengths of 3.6 and 13 cm (*3*). Previous results have been limited to a resolution of about 15 km (the Fresnel zone size at the ring). It is now possible to partially remove the diffraction effects for selected parts of the rings by applying an inverse Fresnel transform to the signal (*7*). The improved resolution is on the order of 1 km, although the data shown below have been smoothed to 10 km resolution.

On Voyager 2, the UVS and PPS instruments simultaneously observed the occultation of δ-Scorpii (HD 143275, B0.5 IV) by the rings. The UVS measured the extinction due to the ring at 1125 Å with a spatial resolution of about